

Layered-Carbon-Stabilized Iron Oxide Nanostructures as Oxidation Catalysts**

Yongjun Gao, Ding Ma,* Gang Hu, Peng Zhai, Xinhe Bao, Bo Zhu, Bingsen Zhang, and Dang Sheng Su*

Dedicated to the Fritz Haber Institute, Berlin, on the occasion of its 100th anniversary

Iron and iron oxide nanoparticles are emerging as promising materials for applications in information recording, magnetic fluids, drug delivery, in-vivo magnetic imaging, and catalysis.^[1–4] In catalysis, it is highly desirable to find cheap replacements for the expensive noble-metal catalysts, such as platinum. One successful example is the development of iron-based nanoparticles which have proven to be highly active catalysts in heterogeneous catalytic oxidation,^[3] hydrogenation,^[5] and C–C bond coupling^[6] reactions. It is well established that the composition, structure, and size control their properties.^[3] The common approaches to fabricate the nanoparticles include the reduction of iron salts,^[7] the reverse micelles method,^[8] and the thermal and reductive decomposition of organometallic iron precursors.^[9] However, most of those methods require surfactants or capping agents, such as oleylamine or oleic acid. Owing to the strong screening effect of such molecules, the reactants will only have limited access to the surface of catalyst particles.

It has been recently demonstrated that layered carbon materials are very promising for applications as catalytic materials because of the unique π -conjugated electron system and the high surface area.^[10–12] It is reported that a three-dimensional (3D) macrostructure composed of noble-metal

nanoparticles (e.g. Au, Ag, Pd, Ir, Rh, or Pt) and graphene single layers can be achieved by controlled assembly using proteins as the attaching agent,^[13] though the efficient control over the structure and size of the nanoparticles still remains a challenge owing to the surface heterogeneity of the graphene/graphene oxide flakes.^[13]

Recently, we reported the preparation of supported organometallic compounds with a π -electron system, such as ferrocene (Fc) on layered carbon materials.^[14] The process was driven by a strong π – π interaction between the guest molecules and the layered carbon. Based on this sandwich-like material we herein present a general method, by which iron/iron oxide nanoparticles with different sizes and structures can be synthesized in situ on the layered carbon materials. Hollow iron oxide nanoparticles with smaller particle sizes can be obtained at relatively low temperatures while a higher preparation temperature leads to the formation of larger-sized core–void–shell complex nanoparticles. It is proposed that the competition/equilibrium between the nucleation and oxidation behaviors of iron under different conditions over the layered carbon materials results in the formation of nanoparticles with different structures. The complex materials obtained are a good replacement for noble-metal catalysts. They demonstrate a high selectivity in catalyzing the oxidation of secondary alcohols.

The oxide-form of layered carbon (OLC) materials (or graphene oxide) was prepared by using a modified Hummer's method with natural flake graphite as the carbon source.^[15] The obtained OLC is rich in oxygen-containing groups, and has a (002) reflection at 11.2°, in the powder X-ray diffraction pattern, corresponding to a *d*-spacing of 0.7 nm which is roughly double the spacing of pristine graphite (Figure 1A). Nitric acid was added to the ferrocene solution, followed with the addition of OCL under stirring. After stirring at room temperature for 24 h, the slurry was filtered, washed, and dried. The material is denoted in the following as Fc-OLC. As the neutral ferrocene molecules became positively charged (ferrocenium cations) when nitric acid was added to the mixture, the electrostatic interaction between the negatively charged surface of the OLC and the positively charged ferrocenium induce absorption/insertion of the ferrocenium onto/into OLC. This process is additionally enhanced by the π – π interaction between the molecules and layered carbon. Inductive coupled plasma emission spectrometer (ICP) analysis shows a Fe content of about 4 wt % (equivalent to a ferrocenium content of about 12.8 wt %) in the Fc-OLC composites while no peak ascribed to the ferrocenium can be

[*] Y. Gao, Prof. Dr. X. Bao

State Key Lab of Catalysis, Dalian Institute of Chemical Physics
Chinese Academy of Sciences, Dalian 116023 (China)

Y. Gao, Prof. Dr. D. Ma, P. Zhai

Beijing National Laboratory for Molecular Sciences
College of Chemistry and Molecular Engineering
Peking University, Beijing 100871 (China)
E-mail: dma@pku.edu.cn

Dr. G. Hu

Exponent Inc., Innovation Tower, Suite 30
3850 Jiangnan Blvd. Hangzhou, 310053 (China)

Dr. B. Zhu, Dr. B. Zhang, Prof. Dr. D. S. Su
Department of Inorganic Chemistry
Fritz Haber Institute of the Max Planck Society
Faradayweg 4–6, 14195 Berlin (Germany)
E-mail: dangsheng@fhi-berlin.mpg.de

Prof. Dr. D. S. Su

Shenyang National Laboratory for Materials Science
Institute of Metal Research, Chinese Academy of Science
72 Wenhua Road, Shenyang 110006 (China)

[**] This work received financial support from the Natural Science Foundation of China (20773121) and 973 Project (2011CB201402). We thank the SSRF for providing the beamline.

Supporting information for this article is available on the WWW under <http://dx.doi.org/10.1002/anie.201101737>.

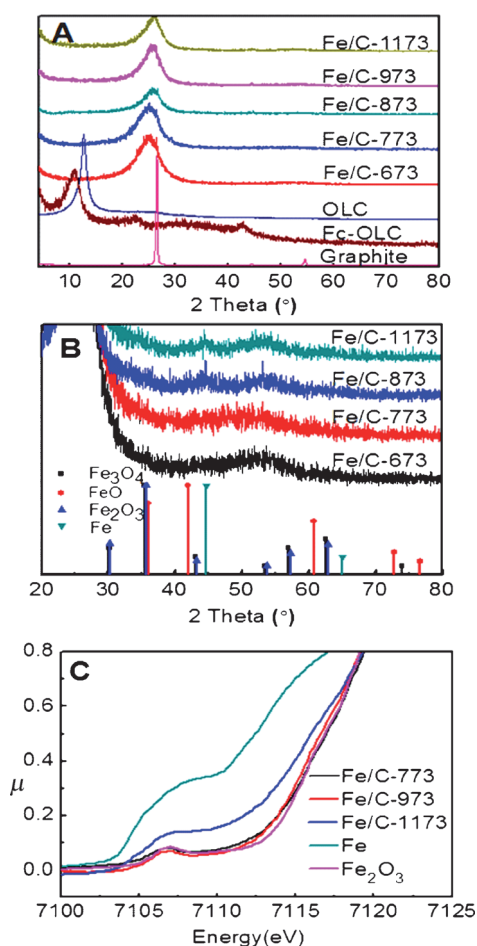


Figure 1. A) Powder XRD patterns of various samples (the numbers in the sample names correspond to the sample treatment temperature); B) magnified XRD profiles; C) Fe K-edge X-ray adsorption spectra of Fe/C catalysts and standard samples.

detected in the XRD profile, suggesting a molecular-level dispersion of ferrocenium over the OLC host (Figure 1A). Moreover, the (002) reflection of Fc-OLC shifted to 10.8° , indicating a swelling of the layers as Fc ions were inserted in between the OLC sheets (Figure 1A).

When the as-obtained Fc-OLC was treated at a high temperature (e.g., 1173 K) under H_2 flow, a matrix of iron/iron oxide nanoparticles dispersed on layered carbon substrate was detected, as shown on a typical SEM image in Figure 2A. TEM (see Figure 2B) clearly shows that the particles are mainly sized in 6–22 nm. It is also noteworthy that those nanoparticles either have a hollow spherical structure or have a core–void–shell complex structure. As the sheets were crumpled in nature, it is hard to tell from the TEM images whether those nanoparticles were on the outer surface of the carbon sheets or in between, while the thickness of the layered carbon is around 2–25 nm (see Figure S1 in Supporting Information).

Crystallographic information regarding the Fe/C samples was detected by XRD. The XRD spectra (Figure 1A) show an shift of the (002) reflection to larger angle for the samples treated at higher temperatures, which, however, is still at a smaller angle than that of pristine graphite. In addition, the

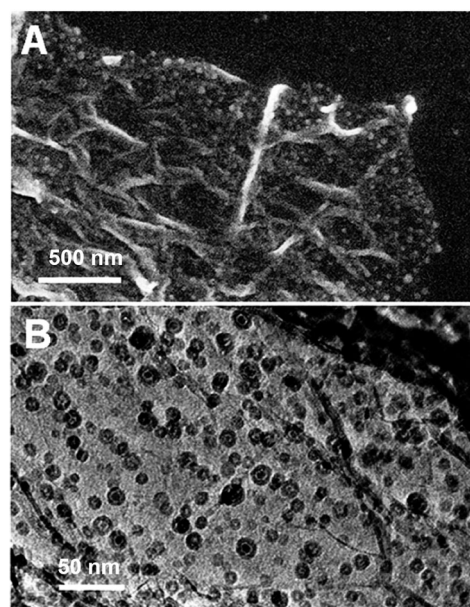


Figure 2. A) SEM and B) TEM images of Fe/C-1173.

reflections remain broad for all Fe/C samples. These results indicate that the interlayer spacing was decreasing when Fc-OLC was treated at elevated temperatures, which is due to the decomposition of oxygen-containing groups in between the OLC layers. The XRD profiles of Fe/C samples only give barely discernible signals at the high-angle range between 35° – 70° (Figure 1B). Referenced to the diffractions of iron species, such signals are most likely associated with iron and iron oxide species. Considering the nano-sized particulate structures shown on electron microscopic images (Figures 2 and 3), we believe the corresponding reflections from iron and iron oxide species are reduced in intensity owing to line broadening, which is a common phenomenon for crystallites in nano-sized range.

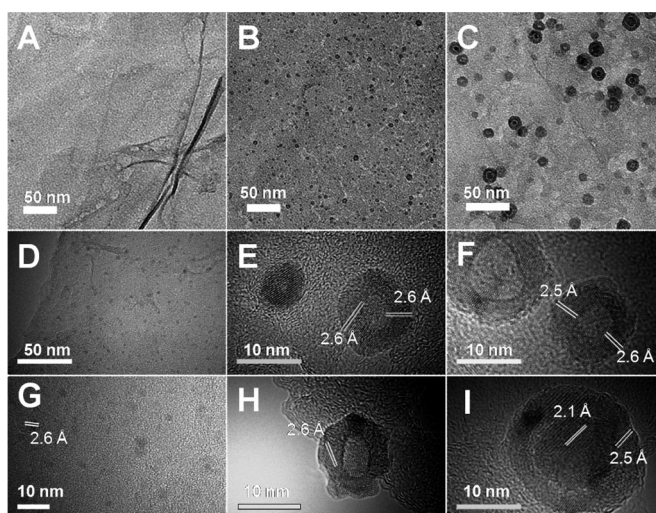


Figure 3. TEM images of OLC (A), Fe/C-873 (B), Fe/C-1173 (C), and Fe/C-773 (D). HRTEM images of Fe/C-773 (G), Fe/C-873 (E,H), and Fe/C-1173 (F,I).

As a further confirmation of the existence of iron species in the Fe/C composites, XAS spectra of these samples clearly resolve Fe K-edge absorption profiles (Figure 1C). For samples from Fe/C-773 and Fe/C-973, the Fe signals are similar with those from iron oxide standard. However, for the sample treated at 1173 K, the pre-edge feature of Fe/C-1173 is in between the features of iron oxide species (Fe_2O_3 or Fe_3O_4) and metallic iron, suggesting the presence of some low valence Fe species in the sample. The treating temperature affected not only the valence state of iron but also the morphological structure of the particles formed on the carbon substrates. The TEM of Fe/C sample prepared at 773 K showed small (around 2 nm on average) particles (Figure 3D and Figures S2 and S3 in the Supporting Information). For sample treated at 873 K, hollow spherical nanoparticles between 4–10 nm were formed (Figure 3B). When the treating temperature reached 1173 K, a mixture of hollow spheres and core–void–shell complex nanoparticles were resulted (Figure 2B and 3C; see also Figure S4–S7 in Supporting Information). The average size of hollow spherical structures is up to 10 nm with a uniform shell thickness of 3–5 nm, whereas the core–void–shell complex nanoparticles have a relatively narrow size distribution around 14–25 nm. The mean shell thickness of these complex structures is around 3–5 nm, while the diameters of the inner cores are ranging widely between 10 nm for the large ones and around 1–3 nm for smaller ones. We observed trenches and holes on the layered carbon for all the Fe/C samples after the nanoparticles were formed. For Fe/C-773, they were barely noticeable, while on Fe/C-873, irregular trenches with a meaning length of 50 nm can be clearly resolved (Figure 3B). Increasing the treatment temperature to 973 K and 1173 K, the trenches merged together and spherical/elliptical holes appeared (see Figure S4 and S6 in Supporting Information). The formation of trenches/holes was a result of the etching of iron/iron oxide nanoparticles during the procedure. This phenomenon is similar to those reported by Johnson et al., where few-layer graphene supported on SiO_2/Si substrate can be etched by thermally activated metallic nanoparticles.^[16]

HRTEM and EELS (electron energy loss spectroscopy) were also used to identify the Fe species in these particulate structures. HRTEM image of Fe/C-773 (Figure 3G) revealed a lattice spacing of 2.6 Å, corresponding to the interplanar distance of (311) planes of $\gamma\text{-Fe}_2\text{O}_3$ or Fe_3O_4 . For the Fe/C-873 sample, similar lattice image was observed, indicating that the hollow spherical particles are polycrystalline iron oxide (Figure 3E and H). For the core–void–shell complex nanoparticles, a typical HRTEM image shows a lattice spacing of 2.1 Å, which can be ascribed to (110) interplanar distance of metallic iron (single crystalline, Figure 3I). Whereas, the HRTEM image of the shell from the same particle shows typical (311) lattice image of the iron oxide species (Figure 3F and I).

The EELS O K-edge profile contains information about the valence state and other structural information of oxygen atoms, so can be used to identify different oxide species. The O K-edge spectra show four typical peaks, labeled a–d in Figure 4, similar to the O K-edge spectra reported by Wang et al.^[17] The O K-edge feature of Fe/C-1173 is similar to the

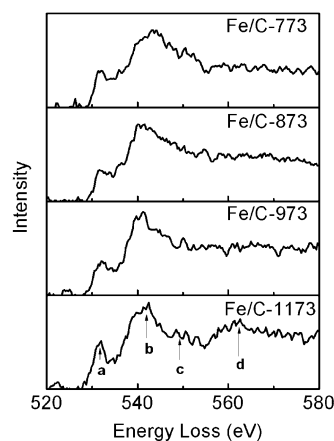


Figure 4. EELS O K-edge spectra of Fe/C-773 (A), Fe/C-873 (B), Fe/C-973 (C), and Fe/C-1173 (D).

spectrum of Fe_3O_4 .^[18,19] Moreover, the intensity ratio of peak a to peak b for Fe/C-1173 is 0.56 which is close to the value (0.57) of core–shell iron oxide particles reported in Wang's work,^[17] however, lower than that of Fe_3O_4 reference (0.69).

This result indicates that the shells of all the samples have a structure similar to that of Fe_3O_4 . And moreover, there were more defects and Fe^{2+} in the oxide shell of the samples than the Fe_3O_4 standard.^[17] The values of a/b of samples Fe/C-773, Fe/C-873, and Fe/C-973 are 0.47, 0.40, and 0.41, respectively (Figure 4). The positions of peaks b and d also reveal information on the defects and Fe–O bond length in the nanostructures.^[17,18] Compared to the Fe_3O_4 standard, the two peaks of as-obtained samples shifted to lower energy range, indicating that there is a higher fraction of Fe^{2+} in the shell and the Fe–O bonding is longer than in Fe_3O_4 . However, based on the pre-edge positions of Fe K-edge X-ray adsorption spectra, it shows that only the valence state of Fe/C-1173 falls in between those of metallic iron and iron oxides. In principle, EXAFS only records an averaged signal from all iron species in bulk, while EELS in conjunction with electron microscopy facilities has a relatively high resolution of different Fe species as it only collects localized information. Therefore, the EELS approach is better to study the core–void–shell Fe/C-1173.

Note that the preparation of core–shell or core–void–shell structures of iron-based nanoparticles has been documented.^[2,17,20–22] However, to date, these complex nanoparticles could only be prepared in liquid and without a support using a precursor decomposition method.^[20] Particles thus obtained have a shell of oxide with a metallic core. The driving force for the formation of the oxide shell is the spontaneous oxidation of metallic iron particles, leading to the formation of a core–shell nanostructure. The further/deeper oxidation of such particles can be realized by increasing the oxidation temperature, creating a very thin low-density region between the inner iron core and the outer oxide shell.^[20] This structure is caused by the coalescence of voids at the interface and is a clear signature of material diffusing forward through the initial oxide shell, leaving the vacancies behind.^[20] Using this nanoscale Kirkendall effect,

Alivisatos et al. were able to prepare monodispersed iron/iron oxide nanoparticles with different structures in a liquid phase system.^[20] In the present study, we believe the formation of various iron-based particulate structures also followed the same general principle although the process could be much more complicated than what happened in liquid phase reactions. Based on our understanding, we propose that the process of integration of the removal of oxygen-containing groups from graphene layers, the decomposition of ferrocene (ferrocenium), and the formation of iron/iron oxide complex nanoparticles, happened sequentially and/or simultaneously. It is reasonable to assume that the nucleation of iron was actually a kinetically controlled process, given that there is a series of complex reactions occurring and that the ferrocenium could be introduced into the OLC sheets of different sizes. Moreover, owing to the surface heterogeneity of layered carbon and the changes during the removal of oxygen-containing groups, the nucleation cannot be as simple as in the liquid phase. Instead, very small iron oxide nanoparticles were first formed (Fe/C-773). With the increase of temperature, driven by the tendency to minimize surface energy, metal nanoparticles tend to agglomerate. As a result, interparticle diffusion and subsequent agglomeration/sintering occurred to form larger particles (Fe/C-873 and Fe/C-1173). The very heterogeneous surface structure of layered carbon determines the diffusion modes of the particles and the formation of structures with different sizes and morphologies. As iron is easily oxidized, upon exposure to air, hollow spheres were obtained (e.g., Fe/C-773 and Fe/C-873) for samples containing relatively smaller particles. In the case of large iron particles, as the rate of oxidation was faster than the rate for iron atoms to diffuse out, a void was formed between the external oxide layer and iron core. Therefore, for samples with larger particles with a wide size distribution, a mixture of hollow spheres and core-void-shell complex nanoparticles were eventually obtained.

The Fe/C composite materials obtained have a relatively large surface area (Table 1), and showed very high activity in catalytic oxidation reactions. Normally, for selective alcohol oxidation, noble-metal catalysts, such as Ru/C,^[23] Pt/C,^[24] Au/TiO₂,^[25] and Pd/SBA-15^[26] are required. As shown in Table 1, when the Fe/C catalysts were used for the oxidation of cyclohexanol at 363 K, all the catalysts showed high selectivity (over 90 %) to ketone, while blank experiments without using catalysts or using reduced graphene oxide as catalyst have a

Table 1: The activity of Fe/C catalysts in the oxidation of cyclohexanol.^[a]

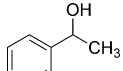
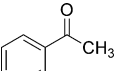
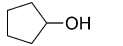
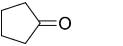
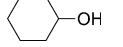
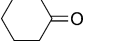
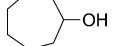
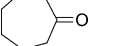
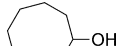
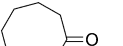
Catalyst	Fe [%] ^[b]	Surface area [m ² g ⁻¹]	Conversion [%]	Selectivity [%]
—	—	—	10.6	64.9
RGO	—	444.1	11.0	71.1
Fe/C-673	3.4	257.0	65.5	89.5
Fe/C-773	3.7	324.9	57.4	92.1
Fe/C-873	3.8	262.1	40.9	90.0
Fe/C-973	3.9	287.1	32.7	90.0
Fe/C-1173	4.2	308.7	20.9	89.7

[a] 5 mmol substrate, 1 mL TBHP (70%), 0.01 g catalyst, and 5 mL CH₃CN as solvent, 363 K, 24 h. [b] Determined by ICP.

relatively low activity and poor selectivity. Among all the catalysts used, Fe/C-673 has the highest activity, which is believed to be related to the relatively small and more uniform particle size. With the particles becoming larger and size distribution wider, the materials exhibited similar selectivity while the conversion decreased dramatically. This study shows that the iron oxide nanoparticles on layered carbon are very active catalysts in catalytic oxidation which was previously a field dominated by precious-metal catalysts.

Our research also shows that these catalysts are generally effective in the oxidation of other secondary alcohols. As shown in Table 2, for all the reactants investigated, the Fe/C composite catalyst showed remarkable performance in conversion and selectivity, demonstrating the potential of this easily prepared, inexpensive, and environmental benign new material in catalytic applications.

Table 2: The activity of Fe/C-673 K catalyst in the oxidation of different secondary alcohols.^[a]

Substrate	Product	Conversion [%]	Selectivity [%]
		98.9	94.1
		55.7	93.9
		65.5	89.5
		76.3	87.0
		70.3	68.4

[a] 5 mmol substrate, 1 mL TBHP (70%), 0.01 g catalyst and 5 mL CH₃CN as solvent, 363 K, 24 h.

In conclusion, layered carbon/iron oxide nano-composites were successfully prepared by a straightforward method. The size and structure of the iron oxide particles embedded in layered carbon can be finely tuned by changing the processing temperature. The procedure is believed to be governed by kinetic-controlled crystallization and oxidation processes, leading to the formation of hollow spherical and core-void-shell nanostructures with different size and void/core diameters. The composite catalysts are very active in catalytic oxidation reactions, even comparable to those of noble-metal catalyst.

Experimental Section

Materials: Natural flake graphite (99.9%) was purchased from LiuMao graphite mine Company. All the other reagents were commercially available, at least of analytical reagent grade and used without further purification.

Preparation of Layered Carbon: The oxide form of layered carbon was prepared with natural flake graphite as the carbon source using a modified Hummer's method.^[15] In a typical procedure, natural flake graphite powder (0.5 g) and sodium nitrate (0.5 g) were added to a flask containing concentrated sulfuric acid (23 mL). The flask was cooled by an ice bath to avoid the temperature of the suspension

exceeding 293 K. KMnO_4 (3 g) was added into the mixture slowly under vigorous stirring. The system was then placed into a water bath (308 K) for 30 min. Distilled water (ca. 46 mL) was slowly added to the suspension and the flask transferred to an oil bath with the temperature controlled at 371 K. 15 min later, the reaction mixture was diluted with distilled water (140 mL) then with H_2O_2 solution (3%; 100 mL) to remove residual KMnO_4 and MnO_2 . The solid product was collected by filtration, washed repeatedly with 5% HCl solution until sulfate could not be detected with BaCl_2 , then washed with water to neutrality, and dried in an air oven at 333 K for 120 h.

Synthesis of Fe/C materials: Ferrocene was loaded into the OLC. Typically, ferrocene (2 g) was added to a 250 mL beaker containing water (20 mL). Concentrated HNO_3 (16 M; 20 mL) was added drop wise into the suspension under fast stirring, a navy blue solution resulted. After adding deionized water (60 mL), a suspension of OLC (0.2 g) in water (100 mL) was added. After stirring at room temperature for 24 h, the suspension was collected by filtration with a membrane filter. The product was washed extensively with water until the filter water is transparent. The product was dried at 333 K for 120 h and then milled into a fine powder. The fine powder (0.1 g) was filled into a quartz tube and the tube was transferred into a fix-bed reactor (i.d. 50 mm) where the sample was fast heated to the designated temperature under H_2 flow (30 mL min^{-1}) and kept at that temperature for 1 min. For example, the product treated at 673 K was denoted as Fe/C-673.

Characterization: Powder X-ray diffraction (XRD) were performed on a RINTD/MAX-2500 X-ray diffractometer using $\text{CuK}\alpha$ radiation ($\lambda = 1.5406 \text{ \AA}$). SEM was recorded on a JSM-6700F field emission scanning electron microscopy (FE-SEM). HRTEM and EELS were conducted in a Philips CM200-FEG, operated at 200 KV, with a Gatan Filter. XPS was performed on an Imaging Photoelectron Spectrometer (Kratos Analytical Ltd.). EXAFS was recorded at the Shanghai Synchrotron Radiation facility. BET measurements were recorded on a Micromeritics ASAP 2010 adsorption apparatus. Before N_2 physisorption measurements all samples were processed at 423 K.

Catalytic Evaluation: Typically, substrate (0.5 g), Fe/C catalysts (0.01 g), TBHP (1 mL, 70%), and CH_3CN (5 mL) were added in turn into a 50 mL round-bottom flask. The flask was placed in an oil bath equipped with a water-cooled condenser. The mixture was heated to a designated temperature under stirring and kept at that temperature for a period of time. 1,4-dioxane (0.5 g) was added to the flask after the reaction as an internal standard for GC analysis. The conversion and selectivity (towards ketone) were determined on an Agilent 7890 GC using an HP-Innowax column.

Received: March 10, 2011

Published online: August 8, 2011

Keywords: core–void–shell particles · heterogeneous catalysis · iron oxide · layered carbon · oxidation

- [1] X. X. Zhang, G. H. Wen, S. M. Huang, L. M. Dai, R. P. Gao, Z. L. Wang, *J. Magn. Magn. Mater.* **2001**, 231, L9–L12.

- [2] Y. Qiang, J. Antony, A. Sharma, J. Nutting, D. Sikes, D. Meyer, *J. Nanopart. Res.* **2006**, 8, 489–496.
 [3] F. Shi, M. K. Tse, M. M. Pohl, A. Bruckner, S. M. Zhang, M. Beller, *Angew. Chem.* **2007**, 119, 9022–9024; *Angew. Chem. Int. Ed.* **2007**, 46, 8866–8868.
 [4] M. M. Mojtahedi, M. S. Abaee, T. Alishiri, *Tetrahedron Lett.* **2009**, 50, 2322–2325.
 [5] P. H. Phua, L. Lefort, J. A. F. Boogers, M. Tristany, J. G. de Vries, *Chem. Commun.* **2009**, 3747–3749.
 [6] X. B. Fan, Z. Y. Tao, C. X. Xiao, F. Liu, Y. Kou, *Green Chem.* **2010**, 12, 795–797.
 [7] M. J. Bonder, Y. Zhang, K. L. Kiick, V. Papaefthymiou, G. C. Hadjipanayis, *J. Magn. Magn. Mater.* **2007**, 311, 658–664.
 [8] M. D. Shultz, W. Braxton, C. Taylor, E. E. Carpenter, *J. Appl. Phys.* **2009**, 105, 07A522.
 [9] S. Peng, C. Wang, J. Xie, S. H. Sun, *J. Am. Chem. Soc.* **2006**, 128, 10676–10677.
 [10] S. Stankovich, D. A. Dikin, G. H. B. Dommett, K. M. Kohlhaas, E. J. Zimney, E. A. Stach, R. D. Piner, S. T. Nguyen, R. S. Ruoff, *Nature* **2006**, 442, 282–286.
 [11] A. K. Geim, K. S. Novoselov, *Nat. Mater.* **2007**, 6, 183–191.
 [12] G. M. Scheuermann, L. Rumi, P. Steurer, W. Bannwarth, R. Mulhaupt, *J. Am. Chem. Soc.* **2009**, 131, 8262–8270.
 [13] J. B. Liu, S. H. Fu, B. Yuan, Y. L. Li, Z. X. Deng, *J. Am. Chem. Soc.* **2010**, 132, 7279–7281.
 [14] Y. J. Gao, G. Hu, W. Zhang, D. Ma, X. H. Bao, *Dalton Trans.* **2011**, 40, 4542–4547.
 [15] W. S. Hummers, R. E. Offeman, *J. Am. Chem. Soc.* **1958**, 80, 1339–1339.
 [16] S. S. Datta, D. R. Strachan, S. M. Khamis, A. T. C. Johnson, *Nano Lett.* **2008**, 8, 1912–1915.
 [17] C. M. Wang, D. R. Baer, J. E. Amonette, M. H. Engelhard, J. Antony, Y. Qiang, *J. Am. Chem. Soc.* **2009**, 131, 8824–8832.
 [18] C. Colliex, T. Manoubi, C. Ortiz, *Phys. Rev. B* **1991**, 44, 11402–11411.
 [19] Z. Y. Wu, S. Gota, F. Jollet, M. Pollak, M. GautierSoyer, C. R. Natoli, *Phys. Rev. B* **1997**, 55, 2570–2577.
 [20] A. Cabot, V. F. Puentes, E. Shevchenko, Y. Yin, L. Balcells, M. A. Marcus, S. M. Hughes, A. P. Alivisatos, *J. Am. Chem. Soc.* **2007**, 129, 10358–10360.
 [21] M. D. Fan, P. Yuan, J. X. Zhu, T. H. Chen, A. H. Yuan, H. P. He, K. M. Chen, D. Liu, *J. Magn. Magn. Mater.* **2009**, 321, 3515–3519.
 [22] S. Peng, S. H. Sun, *Angew. Chem.* **2007**, 119, 4233–4236; *Angew. Chem. Int. Ed.* **2007**, 46, 4155–4158.
 [23] S. Mori, M. Takubo, K. Makida, T. Yanase, S. Aoyagi, T. Maegawa, Y. Monguchi, H. Sajiki, *Chem. Commun.* **2009**, 5159–5161.
 [24] Y. H. Ng, S. Ikeda, T. Harada, Y. Morita, M. Matsumura, *Chem. Commun.* **2008**, 3181–3183.
 [25] J. Ni, W. J. Yu, L. He, H. Sun, Y. Cao, H. Y. He, K. N. Fan, *Green Chem.* **2009**, 11, 756–759.
 [26] C. L. Li, Q. H. Zhang, Y. Wang, H. L. Wan, *Catal. Lett.* **2008**, 120, 126–136.